DFT Investigation of Metal Complexes Containing a Nitrosyl Ligand. 1. Ground State and Metastable States

P. Boulet,[†,‡] M. Buchs,[§] H. Chermette,[*,‡] C. Daul,[§,#] F. Gilardoni,[||] F. Rogemond,[⊥] C. W. Schläpfer,[§] and J. Weber[†]

Université de Genève, département de Chimie Physique, 30 quai E-Ansermet, CH-1211 Genève 4, Switzerland, Université Claude Bernard Lyon 1, Laboratoire de Chimie-Physique Théorique, Bât 201, 43 Bd du 11 novembre 1918, 69622 Villeurbanne Cedex, France and Institut de Recherches sur la Catalyse, CNRS UPR 5401, 69626 Villeurbanne Cedex, France, Institut de Chimie Inorganique, Université de Fribourg, Pérolles, CH-1700 Fribourg, Switzerland, Avantium Technologies, zekeringstraat 29, 1000 CX Amsterdam, The Netherlands, and Laboratoire du Traitement du Signal et Instrumentation, UMR CNRS 5516, Université de Saint Etienne, 23 rue du Dr. P. Michelon, F-42023 Saint Etienne Cedex, France

Received: March 15, 2001; In Final Form: July 9, 2001

Nitrosyl metal complexes, such as the sodium nitroprusside, have attracted chemists' interest for more than 30 years. The existence of long-lived metastable states easily populated by irradiation are the principal reason for this interest. Those long-lived states are interesting either for technical applications or for fundamental research. In this work, we present a comparative density functional theory (DFT) study of the ground state of two different nitrosyl compounds: sodium nitroprusside and cyclopentadienylnitrosylnickel(II).

Introduction

For more than 30 years, nitrosyl transition metal complexes have been extensively studied. The reason for this interest is the presence of long-lived metastable states easily obtained through light irradiation. Complex systems presenting metastable states are good candidates for optical information storage.

Among the nitrosyl complexes, the most studied compound is undoubtedly sodium nitroprusside $Na_2[Fe(CN)_5NO]\cdot 2H_2O$. Its metastable states were discovered in 1977 using Mössbauer spectroscopy.[1] Since the early days and for many years, structure, bonding, and reactivity of nitrosyl transition metal compounds have been the subject of debates and controversies.[2] Following two recent articles dealing with the nitroprusside,[3,4] a consensus has now emerged. However, no ab initio potential energy curve was available so far for the ground state.

The goal of this contribution is to compare theoretically two different nitrosyl compounds, namely, the nitroprusside and the CpNiNO complexes. Our calculations are restricted to the ideal gas-phase situation at 0 K, and the nitroprusside $[Fe(CN)_5NO]^{2-}$ has been considered only in its ionic form. A clear and comprehensive knowledge of the potential energy surface (PES) of these compounds near their ground state is necessary to find the path connecting the ground state (global minimum) to the different metastable states (local minima). It is also of fundamental importance to understand the photochemical behavior of these compounds. A study of the corresponding excited states is the subject of a subsequent paper.[5]

* To whom correspondence should be addressed: cherm@catalyse.univ-lyon1.fr.
[†] Université de Genève.
[‡] Université Claude Bernard Lyon 1.
[§] Université de Fribourg.
[#] E-mail: Claude.Daul@unifr.ch.
[||] Avantium Technologies.
[⊥] Université de Saint Etienne.

Theoretical Approach and Calculation Details

The density functional theory (DFT)[6] within the Kohn and Sham formalism[7] has been used throughout this work at the local density approximation (LDA) and generalized gradient approximation (GGA) levels. The Dirac functional for exchange[8] and the Vosko, Wilk and Nusair[9] (VWN) functional for correlation have been used for the LDA calculations. The Becke[10] exchange functional and the Perdew[11] correlation functional have been used in all gradient corrected calculations (GGA). The combination of these functionals will be hereafter also referred to as B88P86.

The ADF99 program package[12,13] has been employed in all the calculations. A basis set of Slater type orbitals (STOs) taken from ADF basis set IV has been used. It consists of triple-ζ quality atomic orbitals for all atoms augmented by one polarization function. Frozen core potentials were used to model core electrons up to 1s for light atoms and (1s2s2p) for nickel and iron atoms. Finally, according to the ADF99 program conventions, the level of accuracy for the numerical integration has been fixed to 5.0 for optimization procedures and 6.0 for the calculations of vibrational frequencies. Transition states have been fully characterized through the vibration analysis, leading to one imaginary frequency.

Results and Discussion

A. The Nitroprusside Complex. *1. Ground State.* We first performed an optimization of the geometry of the nitroprusside ion, $[Fe(CN)_5NO]^{2-}$, in its ground state. In Table 1, we compare the optimized geometry in C_{4v} symmetry with the experimental crystal structure.[3] As experimental crystals present a small distortion and have a C_s symmetry, two different M−L bond lengths are obtained for the equatorial atoms from the X-ray analysis. This is related to the position of the two counterions in the crystal structure that are neglected in the calculations, as already mentioned.

10.1021/jp010988z CCC: $20.00
Published on Web 09/11/2001

TABLE 1: Structural Parameters of the Ground State of $[Fe(CN)_5NO]^{2-}$ [a]

	LDA	GGA	exp[3]
Fe−N	161.6	164.2	166.56(7)
N−O	115.9	117.0	113.31(10)
$Fe-C_{ax}$	191.5	195.7	192.57(9)
$Fe-C_{eq}$	190.7	195.9	193.10/194.03(6)
$C_{ax}-N_{ax}$	116.4	117.2	115.9(12)
$C_{eq}-N_{eq}$	116.6	117.3	116.03//116.22(8)
$Fe-C_{ax}-N_{ax}$	180.0	180.0	179.78(8)
$Fe-C_{ax}-N_{ax}$	175.0	175.0	178.34/176.49(6)
Fe−N−O	180.0	180.0	176.03(7)
$N-Fe-C_{ax}$	180.0	180.0	176.63(4)
$N-Fe-C_{eq}$	95.2	94.5	93.40/97.65(2)
$C_{eq}-Fe-C_{eq}$(trans)	169.6	171.1	168.91(3)
$C_{eq}-Fe-C_{eq}$(cis)	89.5	89.7	90.25/88.20(2)

[a] Distances in pm.

Our results are in quite good agreement with experimental values and typically in the range of accuracy expected for transition metal compounds with DFT calculations.[14]

It is worthwhile to note that, whereas the Fe−C bond lengths calculated at the LDA level, which were too short by roughly 1.0 to 4.0 pm, are increased by the GGA corrections by 4.0 or 5.0 pm. These corrections also lead to quasi identical $Fe-C_{ax}$ and $Fe-C_{eq}$ bond lengths, whereas the axial experimental bond length is shorter than the equatorial ones. However, the GGA corrections are in the right direction if compared to the LDA bond lengths ($Fe-C_{eq}$ bond lengths are shorter than the $Fe-C_{ax}$ ones). Thus, the GGA corrections do correct insufficiently this discrepancy since they lead to bond lengths almost identical and already too long. Similar effects have been pointed out by Ziegler et al. for various transition metal complexes.[15,16]

Nitroprusside has a $^1A_1$ closed shell ground state, corresponding to an octahedral $t_{2g}^6e_g^0$ occupation. Because of the symmetry, the t_{2g} ligand field orbitals are split into a b_2+e orbitals, and the e_g orbitals are split into a_1+b_1 orbitals (d_{z^2} and $d_{x^2-y^2}$, respectively). The highest occupied molecular orbital (HOMO) is the $2b_2$ orbital and exhibits mainly a d_{xy} iron character. It is almost nonbonding with the CN fragments since the ligand contribution is dominantly located on the N atoms, as depicted in Table 2. In this table, we also see that the lowest unoccupied molecular orbital (LUMO), the 10e, is a π^* antibonding orbital between the iron d_{xy} and d_{yz} atomic orbitals (AOs) and the nitrosyl π^* group. The highest contribution to this orbital stems from the p_x and p_y atomic orbitals of the nitrogen atom of the NO group. This is in agreement with previous DFT calculations.[4]

The MO structure of $[Fe(CN)_5NO]^{2-}$ can easily be rationalized as follow. The interaction between the Fe $d_{xz/yz}$ orbitals and the π_z^* orbitals of equatorial C and N atoms leads in a first step to three MOs, namely, a bonding one (6e), an antibonding one (8e), which is dominantly CN π^* mostly located on N (55%), and an intermediate 7e. In a second step, the symmetry of these e orbitals allows some interaction with the axial CN ligand, leading to a stabilization of the 7e orbital. In addition, this interaction leads to a new, destabilized 9e orbital, with a large axial $\pi_{x/y}^*$ CN character. Finally, in a third step, the interaction with the axial NO ligand leads to a stabilization of the 8e molecular orbital (MO) and an antibonding 10e with a large $\pi_{x/y}^*$ NO character (70%), which is the LUMO. The 8e and 9e MOs, involving the same ligands (CN) lie close in energy, as expected. The LUMO 10e π^* orbital lies, in energy, between the pseudo octahedral t_{2g} and e_g metallic orbitals. This is a general scheme for the nitrosyl compounds[17] and the reason for their interesting properties.

2. Metastable States. Nitrosyl compounds are known for possessing metastable states. This property has been discovered in 1977 in the case of nitroprusside.[1]

The existence of two metastable states originates from the peculiar ground-state potential of the nitroprusside.[3] Starting from the nitroprusside ground state with C_{4v} symmetry, where Fe−N−O atoms are aligned, the molecule can undergo an internal rotation of the nitrosyl group and lead to a first metastable MS_{II} state with C_s symmetry, where Fe−N−O atoms exhibit an angle of 80°. Further on the PES exhibits a second metastable state, MS_I, where Fe−O−N atoms are aligned. This second metastable state has C_{4v} symmetry (cf. Figure 1). Optimized geometrical parameters as compared to experimental geometry, for both metastable states, can be found in Table 3 and Table 5.

For both the MS_{II} and MS_I metastable states, the calculated geometrical parameters are in good agreement with experimental ones. It is worthwhile to note that GGA performs better than LDA.

Both metastable states are ^1A closed shell states, $^1A'$ in case of MS_{II} and $^1A_1$ for MS_I, respectively. In this sense, both of them belong to the potential energy surface of the nitroprusside ground state.

A description of the frontier orbitals of both MS_{II} and MS_I can be found in Table 4 and Table 6, respectively. The HOMO of the MS_I is the $2b_2$ orbital with the major contribution from the d_{xy} atomic orbital from the iron atom. In both the ground state and the MS_I metastable state, the symmetry is C_{4v}. The *z*-axis is the C_4 axis and the *x* and *y* axis are in the direction of the CN groups.

The MS_{II} metastable state possesses only C_s symmetry. In this case, the σ_h symmetry plane contains the iron atom, the nitrosyl group, and three cyano groups. The *z*-axis is perpendicular to this plane. The system of coordinates has undergone a rotation of 90° along the *x*-axis, as compared to the ground state and the MS_I metastable state of nitroprusside. Thus, the HOMO (12a″) is now mainly of d_{xz} character instead of being

TABLE 2: Orbital Contribution to the MOs of the Nitroprusside Ground State[a]

		Fe					N_{NO}		O		C_{ax}		N_{ax}		C_{eq}		N_{eq}	
levels (occup)	energy (eV)	$d_{x^2-y^2}$	d_{z^2}	d_{xy}	d_{xz}	d_{yz}	s	p	s	p	s	p	s	p	s	p	s	p
$5b_1(0)$	−1.71	46													36	14		
$13a_1(0)$	−2.10		49				6				15				14			
$10e_\theta(0)$	−3.65			27				45		24								
$10e_\epsilon(0)$	−3.65					27		45		24								
$2b_2(2)$	−5.63			69														26
$9e_\theta(2)$	−6.52											15		35	7	7		18
$9e_\epsilon(2)$	−6.52										7	22		35	7	7		18
$8e_\theta(2)$	−6.59				28			6		8						16		39
$8e_\epsilon(2)$	−6.59					28		6		8						16		39

[a] In %.

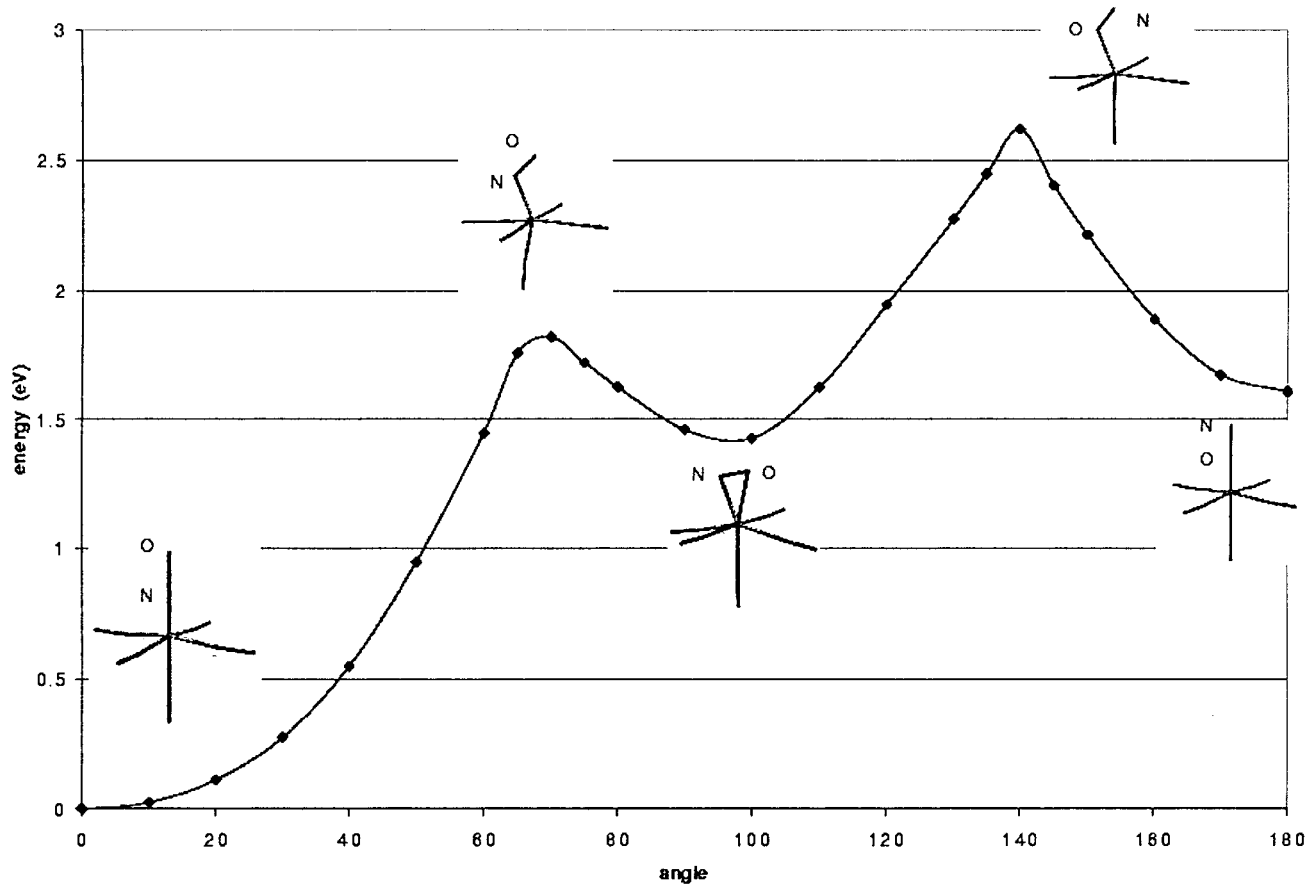

Figure 1. Potential energy curve between Fe−N−O and Fe−O−N.

TABLE 3: Structural Parameters of the MS_{II} of $[Fe(CN)_5NO]^{2-}$[a]

	LDA	GGA	exp[3]
Fe−N	179.4	183.4	189.3(19)
Fe−O	198.9	205.7	206.7(15)
N−O	120.4	121.0	114.(2)
Fe−C(1)	187.1	191.7	182.0(13)
Fe−N−O	80.5	82.2	82.0(13)
N−Fe−C(1)	155.6	155.3	158.7(6)

[a] Distances in pm.

d_{xy}. However, in principle, it is almost the same orbital. This can be seen in Figure 2.

3. Potential Energy Curve. In Figure 1, the potential energy curve which connects together the three minima (the ground state and the two metastable states) is depicted. The angle on the *x*-axis corresponds to the difference between 180° and the value of the Fe−N−O angle.

Relative energies between the ground state, MS_{II} and MS_I, have been calculated to be 1.421 and 1.608 eV, respectively. In the previous paper of Delley,[4] the same relative energies have been calculated to be 1.368 and 1.677 eV. The difference, which is rather small, originates from the nature of the exchange-correlation functional (his GGA is Perdew-Wang91) and the basis sets retained for the calculations. Experimentally, those relative energies are known to be 1.0 and 1.1 eV.[18] The experimental activation energies are also known.[19] E_{a2}, the activation energy for MS_{II} to return to the ground state is 0.5 eV, and E_{a1}, the activation energy for MS_I to go back to MS_{II}, is 0.7 eV. Our calculations lead to 0.39 and 1.19 eV for E_{a2} and E_{a1}, respectively.

The behavior of the frontier orbitals and their main contributions are drawn in Figure 2. In the C_s system of axes, the HOMO remains essentially d_{xz} all along the way. This d_{xz} orbital in C_s symmetry becomes d_{xy} in C_{4v} symmetry, as it is in the case for

TABLE 4: Orbital Contribution to the MOs of the Nitroprusside MS_{II}[a]

		Fe					N_{NO}		O		C_{ax}		N_{ax}		C_{eq}		N_{eq}	
levels (occup)	energy (eV)	$d_{x^2-y^2}$	d_{z^2}	d_{xy}	d_{xz}	d_{yz}	s	p	s	p	s	p	s	p	s	p	s	p
28a′(0)	−1.69		42													28		
27a′(0)	−1.82	33		7				14			12				12			
26a′(0)	−3.52	8		28				17		21								
13a″(0)	−4.24				9	8		56		26								
12a″(2)	−5.47				39	33				9								17
11a″(2)	−5.87				21	31		6		9				5				16
25a′(2)	−6.21											10		27				28
10a″(2)	−6.48											8		19	10	9		35
9a″(2)	−6.69															32		64
24a′(2)	−6.73			16				9		9		9		15		8		20

[a] In %.

TABLE 5: Structural Parameters of the MS_I of $[Fe(CN)_5NO]^{2-a}$

	LDA	GGA	exp[3]
Fe−O	169.7	173.1	117.5(5)
O−N	115.1	116.3	114.0(7)
$Fe-C_{ax}$	187.5	192.1	192.6(6)
$Fe-C_{eq}$	190.6	196.0	194.0/194.7(4)
$C_{ax}-N_{ax}$	116.6	117.2	114.9(7)
$C_{eq}-N_{eq}$	116.8	117.5	115.4/116.1(4)
$Fe-C_{ax}-N_{ax}$	180.0	180.0	179.3(4)
$Fe-C_{ax}-N_{ax}$	175.2	175.5	178.6/176.6(3)
Fe−O−N	180.0	180.0	174.9(4)
$O-Fe-C_{ax}$	180.0	180.0	177.1(3)
$O-Fe-C_{eq}$	94.3	93.6	93.0/97.0(2)
$C_{eq}-Fe-C_{eq}$ (trans)	171.3	172.9	170.0(3)
$C_{eq}-Fe-C_{eq}$ (cis)	89.7	89.8	90.1(2)/88.5(1)

[a] Distances in pm.

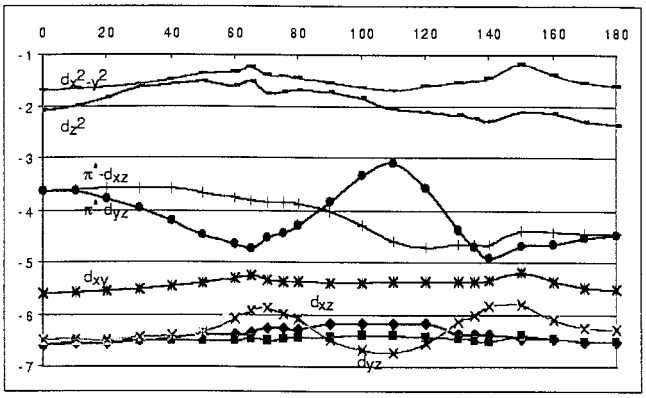

Figure 2. Walsh diagram of the frontier molecular orbitals along the Fe−N−O ↔ Fe−O−N potential energy curve.

the angles of 0° and 180° (see Table 2 and Table 6). Comparing Figure 1 and Figure 2 suggests that the main contribution to the stability is due to the interactions between the occupied d_{xy} orbital and the nitrosyl moiety. This interaction is maximal when the angle Fe−N−O is 0° or 180°, as well as when the angle Fe−N−O is almost 80°, namely, when the nitrosyl group is more or less parallel to the equatorial plane. However, the interaction is of π type in the 0° and 180° cases, whereas it is of σ type in the 80° case.

The CpNiNO Complex. *Structural Parameters and Electronic Structure.* The CpNiNO complex has been fully optimized in C_{5v} symmetry. The structural parameters are reported in Table 7. Our calculated values lie within the range of experimental error estimates. These good results are further confirmed by the predicted NO vibrational frequency (1815 cm^{-1}) as compared with the experimental one (1824 cm^{-1} in hexane matrix).[20]

The electronic configuration of the CpNiNO complex is $5e^4{}_1$-$9a^2{}_1 3e^4{}_2 6e^4{}_1 7e^0{}_1 4e^0{}_2 10a^0{}_1$. This is slightly different from a ZINDO calculation[20] which exhibits an inversion between the $9a_1$ and the $6e_1$ MOs but in full agreement with previous DFT investigations.[21] The composition of the MOs around the Fermi level in terms of AO's contributions are depicted in Table 8. Both the HOMO ($6e_1$) and the LUMO ($7e_1$) exhibit large ligand characters. However, the HOMO has greater C p_π character, whereas the NO π^* mainly contributes to the LUMO. Both of these MOs have a non-negligible nickel d_{xz} AO contribution. The $3e_2$ and the $4e_2$ MOs are highly localized on the Ni atom and the cyclopendienyl (Cp) ligand (π^* AO's), respectively. Finally, as expected, the $9a_1$ MO mainly accommodates the nickel d_{z^2} AO, although a small overlap with the N 2s AO can be noticed.

2. Potential Energy Surface. The PES of the CpNiNO complex is depicted on Figure 3. The origin of the curve is set at the ground-state CpNiNO complex. The PES consists of the ground state (GS) and two local minima (MS_{II} and MS_I) at increasing energy with respect to the Ni−N−O bond angle. The angle is measured between the Ni atom, the center of the NO bond, and the nitrogen atom. These minima are connected together on the PES by two transition states (TS_{II} and TS_I). All the structures are of C_s symmetry except the CpNiNO and CpNiON complexes which belong to the C_{5v} symmetry group. In Figure 4, a Walsh diagram including the MOs around the Fermi level, as a function of the previously defined rotation angle, is depicted. The descent in symmetry from C_{5v} to C_s implies the splitting of the 2-fold degenerate MOs that belong to the irreducible representations (irreps) E_1 and E_2. Both the e_1 and e_2 MOs of the C_{5v} point group give one a″ and one a′ irreps. However, for sake of clarity, only the labels of the C_{5v} point group have been retained on Figure 4. The structures of Figure 3 are repeated in Figure 4 by means of the symbols on the Walsh diagram. Table 9 gathers the electronic contribution of the Ni, N, O, and Cp fragments into the MOs near the Fermi level along the PES.

It can be seen that for the ground state (GS), the $6e_1$ orbital is the HOMO, and it is mainly of Cp character (Table 9). The LUMO is the $7e_1$ MO with NO character. Furthermore, the HOMO-1 is mainly of Ni character with a small contribution of the Cp fragment, whereas, on the contrary, the LUMO+1 exhibits a Cp character with a little contribution from the Ni atom.

The first transition state (TS_{II}) lies 1.44 eV higher in energy than the ground state. It has a bond angle of 43.8° (see Figure 3). One observes that the HOMO splits and is higher in energy than for the GS since the rotation of the NO group decreases the bonding character of the MO between the N and the Ni centers. On the contrary, the LUMO of TS_{II} diminishes its energy as a consequence of the stabilization of the antibonding character of the MO between the N and the Ni atoms (see Figure 4). It is observed that the electron density of the HOMO moves

TABLE 6: Orbital Contribution to the MOs of the Nitroprusside MS_I[a]

		Fe					N_{NO}		O		C_{ax}		N_{ax}		C_{eq}		N_{eq}	
levels (occup)	energy (eV)	$d_{x^2-y^2}$	d_{z^2}	d_{xy}	d_{xz}	d_{yz}	s	p	s	p	s	p	s	p	s	p	s	p
$5b_1(0)$	−1.60	46													36	14		
$13a_1(0)$	−2.38		54								14				12			
$10e_\theta(0)$	−4.46				25			47		26								
$10e_\epsilon(0)$	−4.46					25		47		26								
$2b_2(2)$	−5.54			70														26
$9e_\theta(2)$	−6.30				41			18						8		6		19
$9e_\epsilon(2)$	−6.30					41		18						8		6		19
$8e_\theta(2)$	−6.55											10		24	8	14		31
$8e_\epsilon(2)$	−6.55											10		24	8	14		31

[a] In %.

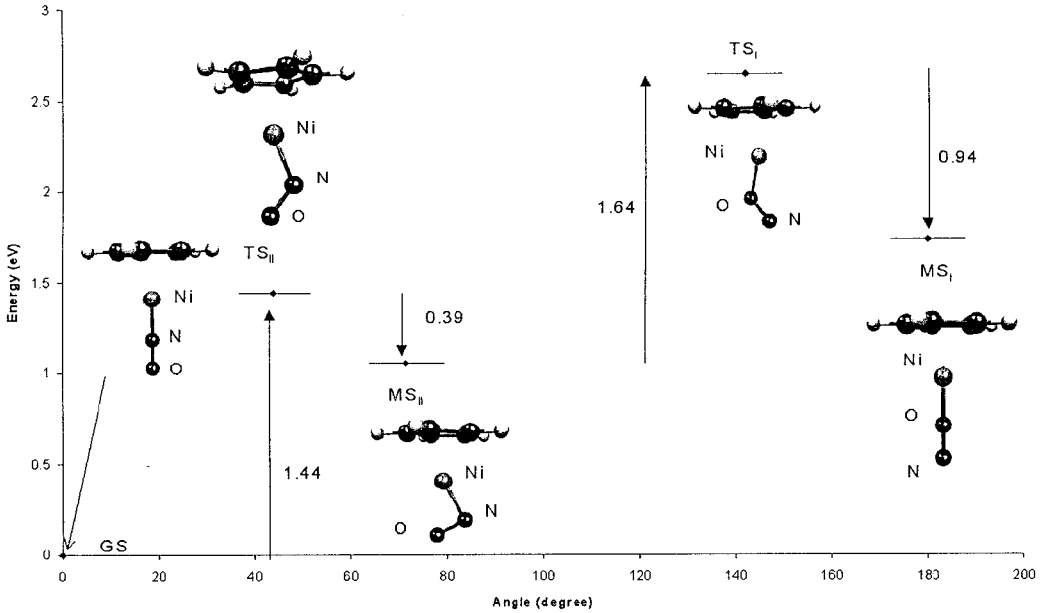

Figure 3. Potential energy surface of the ground-state CpNiNO complex. The angle is measured between the Ni atom, a ghost atom located in the middle of the NO bond, and the N atom.

TABLE 7: Optimized Structural Parameters of CpNiNO Complex − C_{5v} Symmetry[a]

	LDA	B88P86	B88P86[21]	exp
NiC	207.6	214.3	211.8	215 ± 2[20]
NiN	160.5	162.9	163.7	165 ± 3[20]
NiO	277.2	281.0	281.5	278 ± 4[20]
NO	116.7	118.1	117.8	113 ± 7[20]
CH	108.9	108.6	108.8	
NO stretching (cm^{-1})	1899	1815	1845	1824[20]
NiN stretching (cm^{-1})	685	622		636−644[20]
NiNO bending (cm^{-1})	508	472		489−492[23]

[a] Bond lengths in pm.

toward the metal center at the expense of the NO ligand. The Cp contribution is still high, although somewhat reduced. The LUMO orbital is significantly perturbed as the electron density on the Cp fragment drops to almost zero. The corresponding loss of electron density is spread over the metal center and the NO ligand. The density of the HOMO-1 undergoes a significant rearrangement. Both ligand characters increase, whereas that of the Ni atom falls deeply. Finally, the LUMO+1 orbitals is largely relocalized on the NO fragment with a small contribution of the Ni atom, again at the expense of the Cp ligand. The energetics of the latter orbitals are not significantly different from those of the GS species (Figure 4).

The local minimum (MS$_{II}$), located at 71.6°, is 0.39 eV lower than the transition state. This angle corresponds roughly to what

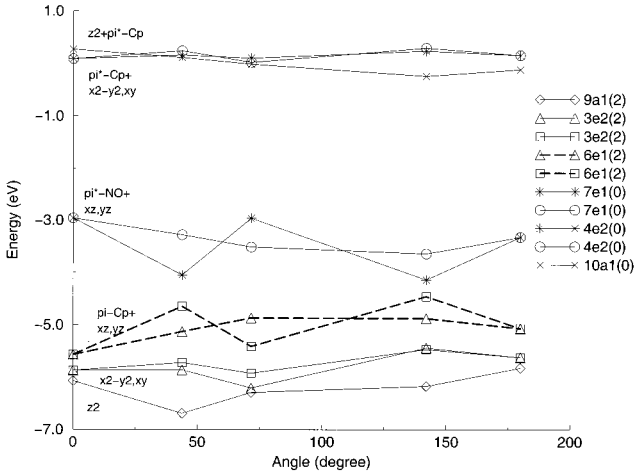

Figure 4. Walsh diagram of the frontier molecular orbitals along the Ni−N−O ↔ Ni−O−N potential energy curve. Labels of the C_{5v} point group has been retained although the molecule falls in C_s symmetry for structures at 43.8°, 71.6°, and 142.0°. The numbers in parentheses correspond to the occupation numbers.

Coppens et al.[22] have already found using the B3LYP functional (88°). At 20 K, it is expected that if the complex is trapped in this well, it cannot overcome this barrier by thermal excitation only. The HOMO-1 and HOMO orbitals crosses each other similarly to the LUMO and LUMO+1. The HOMO and

TABLE 8: MO Composition of CpNiNO − C_{5v}[a]

		Ni					N			O			C			H		
levels (occup)	energy (eV)	s	p	d_{xz}	$d_{x^2-y^2}$	d_{z^2}	s	p_σ	p_π	s	p_σ	p_π	s	p_σ	p_π	s	p_σ	p_π
$10a_1(0)$	0.27	42				2							−11			67		
$4e_2(0)$	0.09				4										91			5
$7e_1(0)$	−2.96			26					39			22			12			
$6e_1(4)$	−5.57		9	13					12			16			47			2
$3e_2(4)$	−5.87				96										4			
$9a_1(2)$	−6.08	11	3			77	4	1		1						1		
$5e_1(4)$	−7.50		1	52					1			7	1	4	29	2		
$2e_2(4)$	−9.47												1	73		24	1	
$8a_1(2)$	−9.97	9	5				1	1			1			1	80			1
$4e_1(4)$	−10.08			5								1	-2	56	1	38		

[a] In %.

TABLE 9: Electronic Composition of the Molecular Orbitals near the Fermi Level along the Potential Energy Surface[a]

	HOMO-1	HOMO	LUMO	LUMO+1
		Ni		
GS	96($d_{xy,\,x^2-y^2}$)	13($d_{xz,\,yz}$),9($p_{x,\,y}$)	26($d_{xz,\,yz}$)	3($d_{xy,\,x^2-y^2}$)
TS_{II}	29(d_{yz}),16(d_{xz}),6(p_z)	39(d_{xy}),3(d_{z^2},p_y),1($d_{x^2-y^2}$)	13($d_{x^2-y^2}$),10(s),4(d_{xy}),2(p_x)	23(d_{xz}),2(d_{yz})
MS_{II}	27(d_{z^2}),12(d_{xy}),3($d_{x^2-y^2}$)	29(d_{yz}),12(d_{xz}),5(p_z)	16(d_{yz}),3(d_{xz})	29(d_{xy}),5(s)
TS_I	19(d_{xz}),16(d_{yz}),5(p_z)	49(d_{xy}),4(p_y),2(d_{z^2}),1(s)	16($d_{x^2-y^2}$),5(s)	24(d_{xz})
MS_I	96($d_{xy,\,x^2-y^2}$)	24($d_{xz,\,yz}$),6($p_{x,\,z}$)	23($d_{xz,\,yz}$)	78(s)+6(d_{z^2})
		N		
GS	0	12(π^*)	39(π^*)	0
TS_{II}	8(π^*)	5(π^*)	40(π^*)	40(π^*)
MS_{II}	19(π^*)	6(π^*)	49(π^*)	30(π^*)
TS_I	25(π^*)	0	53(π^*)	39(π^*)
MS_I	0	27(π^*)	45(π^*)	3(π^*)
		O		
GS	0	16(π^*)	22(π^*)	0
TS_{II}	10(π^*)	2(π^*)	27(π^*)	20(π^*)
MS_{II}	6(π^*)	13(π^*)	22(π^*)	20(π^*)
TS_I	5(π^*)	0	22(π^*)	19(π^*)
MS_I	0	6(π^*)	20(π^*)	1(π^*)
		Cp		
GS	3(π)	47(π)	12(π)	96(π)
TS_{II}	29(π)	42(π)	1(π)	15(π)
MS_{II}	29(π)	39(π)	9(π)	13(π)
TS_I	29(π)	39(π)	0	15(π)
MS_I	4(π)	37(π)	11(π)	15(π)

[a] In %.

HOMO-1 correspond to in-plane and out-of-plane π overlap interactions, respectively. Upon rotation of the NO group, the π bonding overlap between the N and the Ni atoms becomes a π bonding overlap between both N and O atoms and the metal center, therefore strengthening the bond. As the out-of-plane overlap is less efficient than the in-plane one, the latter overlap involves the crossing of these orbitals. The contrary occurs for the LUMO-1 and LUMO. These orbitals have antibonding characters. As a consequence of the rotation of the NO group, the antibonding characters between the N and the Ni atoms is reinforced by the antibonding interaction between the Ni and the O centers. Since the out-of-plane is less destabilizing, the two orbitals crosses. As for TS_{II}, the nickel atom mainly contributes to the density of the HOMO. Therefore, we observe a redistribution of the electron density between the GS and the MS_{II}, which is largely undertaken in TS_{II}. On the contrary, the electron density of the LUMO still remains on the NO ligand all along the reaction coordinates. Finally, we can see that for the HOMO-1 and the LUMO+1 the rearrangement of the electron densities initiated in TS_{II} is still observable in MS_{II}.

The next structure on the PES is a transition state (TS_I) with an almost inverted NO group of atoms as compared to the GS. The angle along the reaction coordinates amounts to 142.0°. It is worth underlining that the NiNO and NiON angles of TS_{II} and TS_I respectively are close (121.8° and 129.7°, respectively). The barrier between MS_{II} and MS_I amounts to 1.64 eV. Once again, the same orbitals as for TS_{II} do cross. Hence TS_{II} and TS_I have the same electron configuration around the Fermi level (i.e., $9a''^2 18a'^2 19a'^0 10a''^0$). Finally, despite these crossings, we can notice that the composition of the MOs of TS_{II} near the Fermi level does not significantly differ from that of MS_I (Table 10).

The last structure of the PES corresponds to the completely inverted ON group of atoms as compared to GS (i.e., CpNiON). It is a local minimum (MS_I) with C_{5v} symmetry and is 1.74 eV less stable than its isomer CpNiNO. The energy difference between TS_I and MS_I amounts to 0.94 eV. Hence, as for MS_{II}, the barrier is too high to be overcome at 20 K. Concerning the electronic structure, it is slightly different from that of GS: the virtual $10a_1$ MO falls lower in energy than the 2-fold degenerated $4e_2$ MOs. Following the PES between TS_I and MS_I, we can see that the electronic composition of the MOs are significantly perturbed as compared to that of TS_I, and in most cases the MOs resemble that of GS. The main difference stems from the LUMO+1 where the density is transferred from the Cp ligand to the Ni atom when one goes from CpNiNO to CpNiON.

TABLE 10: Relative Energies (in eV) of the Metastable- and Transition-States of the CpNiNO and $[Fe(CN)_5NO]^{2-}$ Complexes

	GS	TS_{II}	MS_{II}	TS_I	MS_I
[IMAGE]$Fe(CN)_5NO$ [IMAGE]	0.0	1.81	1.42	2.80	1.61
CpNiNO	0.0	1.44	1.05	2.68	1.74

C. Comparisons between Both Complexes. From a first inspection of Figures 1 and 3, the potential energy surfaces look similar for the two nitrosylsystems. Indeed, the relative energies of the two inverted structures, namely, the MS_I structures, are rather similar, differing by only 0.13 eV for an energy amounting to ca. 1.65 eV above the GS (Table 10). It should be noted that the MS_I of CpNiON lies higher in energy than MS_I of nitroprusside. Similarly, the location of the intermediate metastable states MS_{II} looks rather similar, but the MS_{II} of CpNiNO is indeed 0.37 eV lower than the one of nitroprusside (1.05 vs 1.42 eV, respectively). The importance of relative energy barrier is essential to understand the physics of these metastable states. The barrier of CpNiNO for the reaction GS $\rightarrow$ MS_{II} is much lower than for the nitroprusside (1.44 vs 1.81 eV) whereas the contrary is observed for the reaction $MS_{II} \rightarrow MS_I$ (1.63 vs 1.38 eV). If one considers now the backward reaction from MS_I to GS via MS_{II}, the energy barrier is 0.94 and 0.39 eV for CpNiNO, respectively, and 1.19 and 0.39 eV for the nitroprusside, respectively. Therefore, the backward reaction is more accessible in the case of the CpNiNO complex. This should involve a more seldom observation of the MS_I state of CpNiNO because of a greater ability to isomerize back to either MS_{II} or GS. Finally, it is worthwhile to note that the second metastable state of the nickel complex has not been experimentally observed for a long

TABLE 11: Hirshfeld and Mulliken Charges Analysis along the Ni−N−O ↔ Ni−O−N and Fe−N−O ↔ Fe−O−N Potential Energy Curves

	GS	TS_{II}	MS_{II}	TS_I	MS_I
			CpNiNO		
Hirshfeld					
Ni	0.26	0.33	0.32	0.30	0.27
Cp	−0.14	−0.22	−0.15	−0.23	−0.17
N	−0.05	−0.05	−0.07	−0.03	−0.06
O	−0.07	−0.06	−0.10	−0.04	−0.04
Mulliken					
Ni	0.10	0.16	0.20	0.22	0.17
Cp	0.04	−0.06	0.03	−0.09	0.02
N	0.06	0.10	0.02	0.05	−0.01
O	−0.20	−0.20	−0.26	−0.19	−0.16
			$[Fe(CN)_5NO]^{2-}$		
Hirshfeld					
Fe	0.04	0.03	0.03	0.03	0.04
CN_{ax}	−0.37	−0.32	-0.31	-0.34	-0.36
CN_{eq}	−1.70	-1.72	-1.72	-1.76	-1.74
N	0.09	0.05	0.03	0.00	-0.02
O	-0.06	-0.03	-0.01	0.06	0.09
Mulliken					
Fe	−0.45	−0.38	−0.43	−0.33	−0.35
CN_{ax}	−0.25	−0.22	−0.22	−0.23	−0.24
CN_{eq}	−1.28	−1.38	−1.28	−1.42	−1.38
N	0.23	0.20	0.15	0.08	-0.02
O	−0.26	−0.21	−0.21	−0.09	−0.01

time. Indeed, it has only been recently reported that this MS_I state has been detected by IR spectroscopy after Ar^+-laser irradiation.[23]

The inversion of the NO group along the path from M-NO to M-ON, where M is the Fe or Ni center, can be rationalized in terms of the charge transfers between the ligands and the metal center. Both the Hirschfeld charges and Mulliken charges analysis are presented in Table 11.

For the CpNiNO complex, the Hirshfeld charge on the nickel atom is basically identical for the GS and the MS_I states. The difference is more pronounced with the Mulliken analysis. From GS to TS_{II}, one can observe a clear charge transfer from the metal center to the Cp ligand. In addition, the global electron density on the NO ligand slightly decreases. Interestingly, in terms of Mulliken charges, the charge depletion is mainly attributed to the N atoms, whereas it is the contrary according to the Hirschfeld ones. Overall, we can assume that a global charge transfer occurs from the NO ligand and Ni center toward the Cp ligand. The geometrical rearrangement between TS_{II} and MS_{II} does not affect the charge on the metal center. Part of the electron density of the Cp ligand is transferred to the NO one, in particular to the oxygen atom, or to the nitrogen one, depending on the type of analysis (see Table 11).

For the nitroprusside compound, both analyses (i.e., Mulliken and Hirshfeld) qualitatively agree with each other as far as the GS → TS_{II} rearrangement is concerned. Along this path, one can see from Table 11 that a charge transfer occurs from the Fe, CN_{ax}, and O centers to the CN_{eq} and N (of NO) ligands. From TS_{II} to MS_{II}, the analyses performed differently. From the Mulliken charges analysis, the electron density is partially retrieved on the Fe center and amplified on the N (of NO) atom at the expense of the CN_{eq} ligands.

In conclusion, from the GS to MS_{II} the electron density moves from the metal center to the N (NO) atom. Furthermore, the CN_{eq} ligands of nitroprusside or of the Cp ligand in CpNiNO serves as an electron reservoir when the system crosses the barrier (TS_{II} species). The behavior of the oxygen atom is different depending on the metal compound. Whereas there is a depletion of electron density on O for nitroprusside, the oxygen slightly accepts electrons in the case of CpNiNO.

For the MS_{II} → MS_I reaction, the same trends are observed. Electrons are withdrawn by the equatorial ligands (in the case of the nitroprusside), or by Cp in case of CpNiNO, when the system reaches the top of the barrier (TS_I species). Then, at MS_I, the density increases mainly on the N atom of the NO ligand and partially on the metal center, at the expense of the CN_{eq} ligands. The consequence is that we observe an inversion of the charges on the NO ligand along the reaction path.

From another point of view, as far as the nitrogen atom is still bonded to the metal center (i.e., GS → MS_{II} reaction), the σ-donation is mainly attributed to the N atom. Consequently, the ligand-to-ligand charge transfer is significantly more important on the oxygen atom. Finally, along the path of MS_{II} to MS_I, the main part of the σ-donation is due to the oxygen atom as it is bonded to the metal center. Therefore, the charge on the nitrogen is higher (in term of absolute values).

Conclusion

Our DFT calculations are in good agreement with the known experiments. Both nitrosyl systems are quite similar since they exhibit two metastable states. Those metastable states result from the rotation of the NO group. The first metastable state (MS_{II}) arises after a rotation of about 80°, whereas the second one comes after a rotation of 180°. In both cases, the energy of the first metastable state is lower than that of the second one. Upon this rotation, there clearly appears to be some important electron transfers. Globally, the density is concentrated on the N atom of the ligand, whereas the charge on the O atom decreases. Consequently, one assists at an inversion of charge on these atoms along the path. Obviously, the Cp ligand of CpNiNO and the CN_{eq} ligands of the nitroprusside promotes this transfer as they play the role of a reservoir of electrons.

To have a clear picture of the mechanism of population of those metastable states, a study of the excited states is of fundamental importance. This problem is tackled in a subsequent article.

Acknowledgment. The authors thank Prof. Andreas Hauser from the University of Geneva for fruitful discussions, as well

as Dr. Eric Furet at the earlier stage of this work. This work is supported by the Swiss National Science Foundation and the COST action D9.

References and Notes

(1) Hauser, U.; Oestreich, V.; Rohrweck, H. D. *Z. Phys. A*, **1977**, *280*, 125.

(2) Bohr, F.; Chermette, H.; Ruiz-López, M. F. *Int. J. Quantum Chem.* **1994**, *52*, 1039.

(3) Carducci, M. D.; Pressprich, M. R.; Coppens, P. *J. Am. Chem. Soc.* **1997**, *119*, 2669.

(4) Delley, B.; Schefer, J.; Woike, T. *J. Chem. Phys.*, **1997**, *107*, 10067.

(5) Boulet, P.; Buchs, M.; Chermette, H.; Daul, C.; Gilardoni, F.; Rogemond, F.; Schläpfer, C. W.; Weber, J. *J. Phys. Chem. A* **2001**, *105*, 8999.

(6) Hohenberg, P.; Kohn, W. *Phys. Rev. A*, **1964**, *136*, 864.

(7) Kohn, W.; Sham, L. J. *Phys. Rev. A*, **1965**, *140*, 1133.

(8) Dirac, P. A. M. *Proc. Cambridge Philos. Soc.* **1930**, *26*, 376.

(9) Vosko, S. H.; Wilk, L.; Nusair, M. *Can. J. Phys.* **1980**, *58*, 1200.

(10) Becke, A. D. *Phys. Rev. A* **1988**, *38*, 3098.

(11) Perdew, J. P. *Phys. Rev. B* **1986**, *33*, 8822.

(12) Baerends, E. J.; Bérces, A.; Bo, C.; Boerrigter, P. M.; Cavallo, L.; Deng, L.; Dickson, R. M.; Ellis, D. E.; Fan, L.; Fischer, T. H.; Fonseca Guerra, C.; van Gisbergen, S. J. A.; Groeneveld, J. A.; Gritsenko, O. V.; Harris, F. E.; van den Hoek, P.; Jacobsen, H.; van Kessel, G.; Kootstra, F.; van Lenthe, E.; Osinga, V. P.; Philipsen, P. H. T.; Post, D.; Pye, C. C.; Ravenek, W.; Ros, P.; Schipper, P. R. T.; Schreckenbach, G.; Snijders, J. G.; Sola, M.; Swerhone, D.; te Velde, B.; Vernooijs, P.; Versluis, L.; Visser, O.; van Wezenbeek, E.; Wiesenekker, G.; Wolff, S. K.; Woo, T. K.; Ziegler, T. *ADF1999*; Scientific Computing & Modelling NV: Amsterdam, 1999.

(13) Fonseca Guerra, C.; Snijders, J. G.; te Velde, B.; Baerends, E. J. *Theor. Chem. Acc.*, **1998**, *99*, 391.

(14) Chermette, H. *Coord. Chem. Rev.* **1998**, *178*−*180*, 699.

(15) Ziegler, T. *Chem. Rev.* **1991**, *91*, 651.

(16) Ziegler, T. *Can. J. Chem.* **1995**, *73*, 743.

(17) Enemark, H.; Feltham, R. D. *Coord. Chem. Rev.* **1974**, *13*, 339.

(18) Zöllner, H.; Woike, T.; Krasser, W.; Haussühl, S. *Z. Kristallogr.* **1989**, *188*, 139.

(19) Woike, T.; Kirschner, W.; Schetter, G.; Barthel, T.; Hyunf-Sang, K.; Haussühl, S. *Opt. Comm.* **1994**, *106*, 6.

(20) Chen, L. X.; Bowman, M. K.; Wang, Z.; Montano, P. A.; Norris, J. R. *J. Phys. Chem.* **1994**, *98*, 9457.

(21) Field, C. N.; Green, J. C.; Mayer, M.; Nastuzov, V. A.; Rösch, N.; Siggel, M. R. F. *Inorg. Chem.* **1996**, *35*, 2504.

(22) Coppens, P.; Fomitchev, D. V.; Carducci, M. D.; Culp, K. *J. Chem. Soc., Dalton Trans.*, **1998**, 865.

(23) Schaiquevich, P. S.; Güida, J. A.; Aymonino, P. J. *Inorg. Chim. Acta*, **2000**, *303*, 277.